Neuron
Article

Retinal Input Directs the Recruitment of Inhibitory Interneurons into Thalamic Visual Circuits

Bruno Golding,[1] Gabrielle Pouchelon,[1] Camilla Bellone,[1] Sahana Murthy,[1] Ariel A. Di Nardo,[4] Subashika Govindan,[1] Masahuro Ogawa,[5] Tomomi Shimogori,[5] Christian Lüscher,[1,2] Alexandre Dayer,[1,3] and Denis Jabaudon[1,2,*]
[1]Department of Basic Neurosciences, University of Geneva, 1 Rue Michel Servet, 1211 Geneva, Switzerland
[2]Department of Neurology
[3]Department of Psychiatry
Geneva University Hospital, 4 Rue Gabrielle-Perret-Gentil, 1205 Geneva, Switzerland
[4]Center for Interdisciplinary Research in Biology, UMR CNRS 7241/INSERM U1050, Collège de France, 11 Place Marcelin Berthelot, 75005 Paris, France
[5]Riken Brain Science Institute, 2-1 Hirosawa Wako City, Saitama 351-0198, Japan
*Correspondence: denis.jabaudon@unige.ch
http://dx.doi.org/10.1016/j.neuron.2014.01.032

SUMMARY

Inhibitory interneurons (INs) critically control the excitability and plasticity of neuronal networks, but whether activity can direct INs into specific circuits during development is unknown. Here, we report that in the dorsal lateral geniculate nucleus (dLGN), which relays retinal input to the cortex, circuit activity is required for the migration, molecular differentiation, and functional integration of INs. We first characterize the prenatal origin and molecular identity of dLGN INs, revealing their recruitment from an *Otx2*$^{+}$ neuronal pool located in the adjacent ventral LGN. Using time-lapse and electrophysiological recordings, together with genetic and pharmacological perturbation of retinal waves, we show that retinal activity directs the navigation and circuit incorporation of dLGN INs during the first postnatal week, thereby regulating the inhibition of thalamocortical circuits. These findings identify an input-dependent mechanism regulating IN migration and circuit inhibition, which may account for the progressive recruitment of INs into expanding excitatory circuits during evolution.

INTRODUCTION

Two broad functional classes of cells, excitatory and inhibitory neurons, form the neuronal circuits of the CNS. Circuits with high levels of excitatory activity require a compensatory inhibition to allow activity-dependent plasticity while avoiding excitotoxicity (Spitzer, 2006; Akerman and Cline, 2007; Miraucourt et al., 2012). Inhibitory interneurons (INs) control the dynamics and temporal limits of this plasticity by regulating the spatial and temporal spread of incoming excitatory signals (Isaacson and Scanziani, 2011), as exemplified during the development of ocular dominance columns in the visual cortex (Hensch, 2005; Hooks and Chen, 2007; Sugiyama et al., 2008; Runyan et al., 2010; Southwell et al., 2010). While recent reports have revealed that the migration and differentiation of specific subtypes of neocortical INs relies partly on cell-intrinsic activity, and that their migration is guided by target-derived factors (López-Bendito et al., 2008; Bortone and Polleux, 2009; De Marco García et al., 2011; Lodato et al., 2011; Miyoshi and Fishell, 2011; Wang et al., 2011a), whether the level or pattern of activity within target neuronal circuits acts to recruit migrating INs during development is unknown. Here, we investigate this possibility by studying the development and integration of INs into visual circuits of the dorsolateral geniculate nucleus (dLGN) of the thalamus, which has a well-characterized input-output connectivity, is comprised of a single type of excitatory projection neuron, and has local INs that form feedforward inhibitory connections. We show that while the initial migration of INs into the dLGN does not rely on circuit activity, their targeted navigation and synaptic integration into dLGN circuits is controlled by retinal input.

Thalamocortical (TC) neurons in the dLGN receive monosynaptic input from retinal ganglion cells and send their axonal output to the visual cortex (López-Bendito and Molnár, 2003). In contrast to other rodent thalamic relay nuclei, which consist exclusively of excitatory TC neurons, the dLGN contains ~20% of local INs, a proportion similar to that found in the neocortex (Arcelli et al., 1997). TC neurons and local INs both receive input from the retina, and feedforward inhibition of TC neurons by dLGN INs controls the transmission of visual signals to the neocortex (Wang et al., 2011b). This inhibition enhances selectivity for stimulus features in space and time and is regulated by cholinergic input from the brainstem, thereby providing a critical precortical filtering of retinal input (Sillito and Kemp, 1983; Berardi and Morrone, 1984; Norton and Godwin, 1992; Hu et al., 2000; Blitz and Regehr, 2005; Wang et al., 2011b, 2011c). Consistent with a prominent role in visual processing, the proportion of dLGN INs to TC neurons increases dramatically in primates, in which hand-eye coordination and stereoscopic and color vision are behaviorally central (Arcelli et al., 1997).

Although dLGN INs were first described by Cajal over a century ago and their functional importance has since been established, their molecular identity and ontology remain largely unknown (Cajal, 2002; Letinic and Rakic, 2001; Jones, 2002; Hayes et al., 2003; Ortino et al., 2003; Bickford et al., 2010). Furthermore, while retinal activity plays a critical role in the retinotopy and eye-specific segregation of retinogeniculate axons (Penn et al., 1998; Hooks and Chen, 2007; Huberman et al., 2008), whether retinal input plays a role in the assembly of local inhibitory circuits in the dLGN is unknown.

In this study, we show that dLGN INs are born from a restricted proliferative niche in the ventral wall of the third ventricle and reside in the vLGN, an ancestral retinal target, until birth. Only postnatally are they progressively recruited into dLGN circuits. Using microsurgical, genetic, pharmacological, and electrophysiological analyses in vitro and in vivo, we show that retinal activity controls the postnatal migration and functional synaptic integration of dLGN INs, thereby acting to regulate TC neuron excitability during a critical period of postnatal development. Together, these findings indicate that retinal activity directs the incorporation of inhibitory neurons into the dLGN, establishing the balance of excitation and inhibition in thalamic visual circuits.

RESULTS

A Molecularly Defined Population of GABAergic INs Migrates into the dLGN during the First Postnatal Week

In order to determine how the inhibitory circuits of the visual thalamus develop, we used GAD67^{GFP} transgenic mice (Tamamaki et al., 2003) to track the distribution of GABAergic INs in the dLGN during development. At birth, while extrathalamic retinal targets such as the ventral lateral geniculate nucleus and intergeniculate leaflet (here collectively referred to as vLGN) already contain large numbers of GFP$^+$ INs, the dLGN only contains very few INs at postnatal day (P) 1 (Figures 1A and 1B). During the first postnatal week, however, GFP$^+$ INs progressively migrate into the dLGN (Figures 1B–1D), initially in the most superficial tier of the dLGN, just below the optic tract, where they appear to be migrating out of the vLGN (Figure 1B, arrowheads), and later into deeper tiers of the nucleus (Figures 1C–1G). This postnatal IN migration is strictly limited to the dLGN, since GFP$^+$ neurons are not found in the adjacent ventral posterior medial (VPM) nucleus (Figures 1A–1E). Therefore, the migration of INs into the dLGN is a progressive process, proceeding from superficial to deeper tiers of this nucleus during the first postnatal week.

In order to investigate the developmental origins of dLGN INs, we next sought to characterize their molecular identity. For this purpose, we used a gene microarray approach in samples collected at P0, P3, and P10 from the dLGN (which is progressively populated by INs) and the VPM (which lacks INs) (Figure 1H). We performed a cluster analysis of the developmental time course of *Gad67* expression to identify putative IN-specific genes. An initial set of 71 genes with GAD67-like expression profiles were identified, which we narrowed down to eight top dLGN IN candidate genes after in silico screening and confirmation of expression by in situ hybridization and immunocytochemistry (Figures 1I–1R″ and S1A– S1F available online). Genes specifically expressed by dLGN INs, but not by dLGN TC neurons, included the transcription factor *Otx2*, which critically controls IN development and plasticity in the visual cortex (Sugiyama et al., 2008), and its binding partner *Meis2* (*Mrg1*) (Agoston and Schulte, 2009) (Figures 1I–1L″), as well as a set of three synaptic proteins: complexin 3 (*Cplx3*), a presynaptic protein that binds SNARE complexes and regulates vesicular release (Reim et al., 2009) (Figures 1M–1N″), and two subunits of postsynaptic nicotinic acetylcholine receptors, $\alpha 6$ and $\beta 3$ (Figures 1O–1R″). Remarkably, in contrast to the vLGN and neocortex, where inhibitory INs belong to distinct molecular subtypes (Gelman and Marín, 2010; Jeong et al., 2011), dLGN INs were molecularly homogenous, i.e., this set of genes was expressed by essentially all INs in this nucleus at P20 (Figures 1I–1R″ and S1G–S1N″; Table 1). This molecular homogeneity is consistent with the largely uniform morphology and physiological properties of these neurons (Williams et al., 1996) and suggests that dLGN INs belong to a single neuronal lineage.

dLGN INs Migrate from the vLGN and Are Born from a Prethalamic Progenitor Microdomain

Expression of the synaptic proteins *Cplx3*, $\alpha 6$ *nAChR*, $\beta 3$ *nAChR*, and *Meis2* is specific to dLGN INs since only a few scattered INs express these genes in the vLGN (Figures S1C–S1E). In contrast, *Otx2* is expressed by both dLGN INs and a subpopulation of vLGN INs (Figures 1I and S1A), suggesting common origins. As a first step to test this hypothesis, we followed the migration of *Otx2*$^+$ INs during embryonic development.

Examining GAD67^{GFP} mice, we found that between embryonic day (E) 12.5 and E18.5, *Otx2*$^+$ INs form a migratory stream between a small region of the ventral wall of the third ventricle (V3) and the ventral part of the vLGN (Figures 2A–2B″; data not shown). This stream is specific to *Otx2*$^+$ INs, since vLGN INs, which express *Tal1* and *Sox14* (Vue et al., 2007; Kataoka and Shimogori, 2008; Scholpp and Lumsden, 2010; Suzuki-Hirano et al., 2011; Delogu et al., 2012), migrate into the vLGN through a distinct, more dorsal pathway (Figures 2C–2D″ and S2A–S2B″). This suggests that *Otx2*$^+$ INs and *Otx2*$^-$,*Tal1*$^+$ vLGN INs belong to distinct lineages. Supporting this distinction, *Otx2*$^-$ *Tal1*$^+$ INs remain in the vLGN postnatally and are not found in the dLGN (Figures S2C and S2D′), while *Otx2*$^+$ INs are found in both the dLGN and vLGN (Figures 1I and S1A).

To further examine whether vLGN and dLGN *Otx2*$^+$ INs have common origins, we fate mapped dLGN INs by electroporating an RFP reporter plasmid in utero at E12.5 into the ventral wall of V3, from where the *Otx2*$^+$ IN stream originates (Figure S2E). When examined at P7, the RFP$^+$ progeny of these cells consisted exclusively of vLGN and dLGN INs (Figures S2F and S2G″), indicating that dLGN INs and subsets of vLGN INs are born together in the ventral V3 neuroepithelium. Furthermore, dLGN TC neurons did not express RFP (Figures S2G–S2G″), nor did dLGN INs express the panthalamic projection neuron marker SOX2, indicating that the ontogeny of dLGN INs is distinct from that of dLGN TC neurons (Figures S2H and S2I″).

Finally, we used a genetic fate-mapping strategy to precisely identify the site of birth of dLGN INs and to confirm the shared lineage relationship of *Otx2*$^+$ dLGN and vLGN INs. Using an in silico screen of genes expressed in the V3 wall during

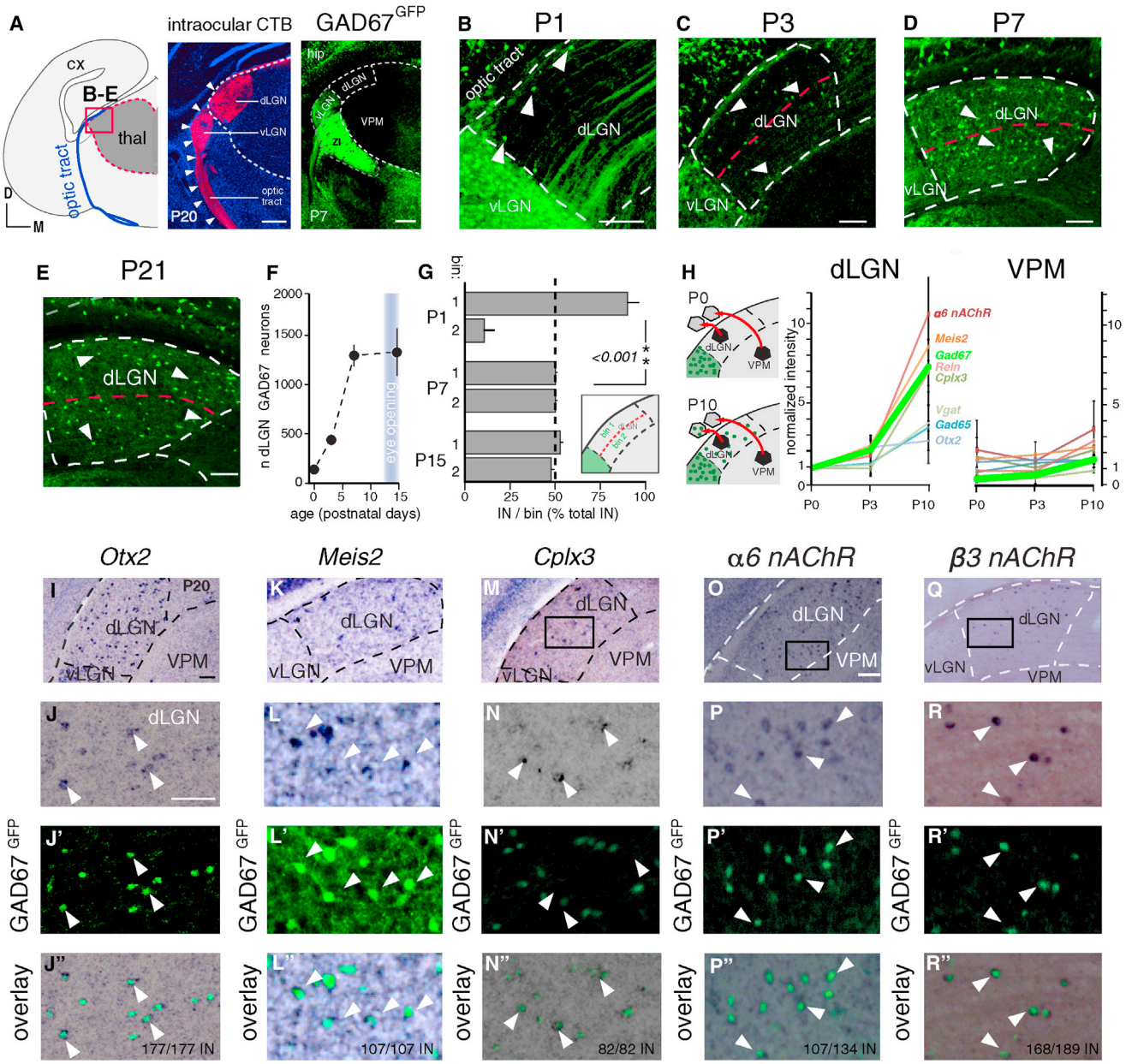

Figure 1. A Molecularly Defined Population of GABAergic INs Migrates into the dLGN during the First Postnatal Week

(A) Left: schematic coronal section showing location of the photomicrographs taken in (B)–(E). Middle: retinal ganglionic cell axons form the optic tract and project to the vLGN and dLGN as revealed by anterograde labeling from the retina. Right: coronal section in GAD67^{GFP} mice showing INs in the prethalamus (vLGN and ZI). Within the thalamus, INs are exclusively found in the dLGN.

(B–E) dLGN INs are initially found in the superficial part of the dLGN, close to the border with the vLGN (B) and then progressively distribute within the dLGN during the first postnatal week (C–E, arrowheads). (C) P3, (D) P7, and (E) P21.

(F) Quantification of postnatal migration of INs into the dLGN.

(G) Developmental distribution of INs within the dLGN. Fisher's exact test, n = 96 P1 and n = 440 P7 INs. Number in italic indicates p value. Inset shows schematic delineation of bin 1 (superficial) and 2 (deep), also represented by the dashed red lines in (C)–(E).

(H–R″) Molecular identity of dLGN INs. (H) Left: microarray experimental principle: INs (green dots) are present in the dLGN at P10 but not P0 and remain absent from the VPM. Right: microarray fluorescence intensity of the transcripts identified by cluster analysis of probes whose expression covaries with *Gad67*. (I–R″) In situ hybridization in GAD67^{GFP} mice confirms IN specificity of the genes identified in (H). Values in (J″), (L″), (N″), (P″), and (R″) indicate proportion of GFP^{+} INs expressing each transcript. Abbreviations: CTB, cholera toxin B; hip, hippocampus; thal, thalamus; dLGN, dorsolateral geniculate nucleus; vLGN, ventrolateral geniculate nucleus; VPM, ventroposterior medial nucleus; ZI, zona incerta. Scale bars represent 250 μm in (A); 100 μm in (B)–(E), (I), (K), (M), (O), and (Q); and 50 μm in (J)–(J″), (L)–(L″), (N)–(N″), (P)–(P″), and (R)–(R″). Values are represented as mean ± SEM. See also Figure S1.

Table 1. Molecular Identity of Thalamic and Prethalamic Interneurons

Gene	RN/ZI	vLGN	dLGN
5HT3a Cre	0	0	0
Calret	0	++	0
Chrna6	0	(+)	+++
Chrnb3	0	(+)	+++
Cplx3	++	(+)	+++
GAD65	++	+++	0
Meis2	++	0	+++
Nkx2.1	0	++	0
Nkx5.1	0	0	0
NPY	++	(+)[a]	0
Otx2	++	+	+++
Parv	++	0	0
Rln	0	+	+++
Sst	++	0	0
VIP	++	0	0

+++, >95% INs express gene; ++, 50%; +, 25%; (+), <10%. RN, reticular nucleus; ZI, zona incerta.
[a]Present in the intergeniculate leaflet (IGL)

development, we found that *Fgf8*$^{+}$ neurons colocalize with *Otx2*$^{+}$ INs along the ventral migratory stream during embryogenesis but that, in contrast to *Otx2*, *Fgf8* expression in progenitor is restricted to a small prethalamic third ventricular domain (Kataoka and Shimogori, 2008) (Figures 2E and 2E′). Since *Fgf8* itself is not expressed in the dLGN (data not shown), we fate mapped the neurons born from this niche using an *Fgf8*^{Cre} transgenic mouse (Toyoda et al., 2010) and found that these progenitors give rise to specific subsets of INs in the vLGN, as well as within the dLGN (Figures 2F and S2J). Together, these findings indicate that dLGN INs are born from a restricted prethalamic progenitor domain and migrate along a dedicated pathway to first reach the vLGN, between E12.5 and E15.5. Only postnatally does a specific subset of *Otx2*$^{+}$ vLGN INs migrate into and distribute within the dLGN (Figure 2G).

Otx2 Function Is Required Postnatally to Establish dLGN Inhibitory Circuits

Otx2^{+} INs initially reach the vLGN at E15.5 and reside in the ventral part of the nucleus before migrating toward the vLGN-dLGN border by approximately E18.5 (Figures 3A and 3B), after which a subset of these neurons exit the vLGN to migrate into the dLGN at P0–P1 (Figure 3C).

We next investigated the molecular mechanisms that allow a subpopulation of *Otx2*$^{+}$ INs to migrate out of the vLGN into the dLGN. Our microarray analyses revealed that *Meis2*, a binding partner and activator of OTX2 function (Figure 3D; Agoston and Schulte, 2009), is specifically expressed by *Otx2*$^{+}$ INs in the dLGN but not the vLGN (Figures 3E and S1B). We therefore hypothesized that OTX2 protein activity might distinguish dLGN and vLGN *Otx2*$^{+}$ INs and examined whether other OTX2-interacting proteins might be differentially expressed in these two populations. Supporting this possibility, we found that TLE4, which binds to and inactivates OTX2 (Figure 3D; Heimbucher et al., 2007; Agoston and Schulte, 2009), is expressed exclusively by vLGN INs (Figure 3F). Therefore, *Meis2*, an OTX2 activator, and TLE4, an OTX2 inhibitor, are mutually exclusively expressed in dLGN and vLGN INs. Therefore, OTX2 might be inactive in the vLGN and become active in the dLGN. To directly test whether OTX2 activation is required for dLGN IN function, we thus used an inducible self-knockout strategy (*Otx2*^{CreERT2}/*Otx2*^{flox}) to postnatally ablate *Otx2* expression specifically in postmitotic *Otx2*$^{+}$ neurons at P0 (Figure S3; Fossat et al., 2006). Such perinatal removal of OTX2 leads to a specific loss of dLGN INs, while vLGN INs were seemingly unaffected (Figures 3G, 3H, and S3). Therefore, OTX2 function is required for INs to migrate into or survive within the dLGN and reveals a critical role for this transcription factor in the assembly of local inhibitory circuits within the visual thalamus.

Retinal Input Directs the Migration and Functional Synaptic Integration of dLGN INs during a Critical Period of Development

Since retinal input is critical for the assembly of retinogeniculate and thalamocortical circuits (Huberman et al., 2008) and paracrine neurotransmitter release regulates the migration of neurons in several brain regions (Manent et al., 2005, 2006; Spitzer, 2006), we hypothesized that the postnatal migration and circuit integration of dLGN INs might be regulated in an input-dependent manner. As a first step to assess a role for neuronal activity in dLGN IN migration, we used in vitro time-lapse imaging of acute coronal brain sections from P1 GAD67^{GFP} mice. We examined whether dLGN IN migration was affected by blocking spontaneous circuit activity using bath application of the voltage-gated sodium channel blocker tetrodotoxin (TTX), which dramatically reduced the migration speed of dLGN INs (Figure 4A). Remarkably, this effect was specific to this IN population, since the migration of nearby hippocampal INs remained unaffected (Figure 4A; $p = 0.002$ for Ctl versus TTX in dLGN INs; $p = 0.94$ for hippocampal INs; paired t test). These results indicate that neuronal activity specifically affects the migration of dLGN INs after birth.

Since TTX could affect IN migration both by cell-autonomous and non-cell-autonomous mechanisms, we next specifically manipulated dLGN input in vivo. Glutamatergic retinogeniculate axons are a primary source of excitatory input to the dLGN, and INs first migrate into this nucleus in close proximity to these axons (Figure 1B), at a time when retinal activity is progressively increasing (Huberman et al., 2008). This suggested to us that retinogeniculate input may play a role in the incorporation of INs into dLGN circuits. To test this possibility, we performed a bilateral optic nerve section (ONS) at birth in GAD67^{GFP} mice and found that lack of retinal input profoundly affected the migration of dLGN INs at P20. While GAD67^{GFP} INs normally migrate into the superficial tiers of the dLGN and then distribute homogeneously within this nucleus (Figures 1B–1D), in the absence of retinal input they remained predominantly located in superficial tiers of the dLGN, where they displayed a seemingly differentiated morphology, and failed to distribute in deeper tiers of the dLGN (Figures 4B–4G). Interestingly, IN migration along the lateromedial axis of the dLGN was unaffected (Figures 4E and 4F), suggesting that different processes regulate the tangential

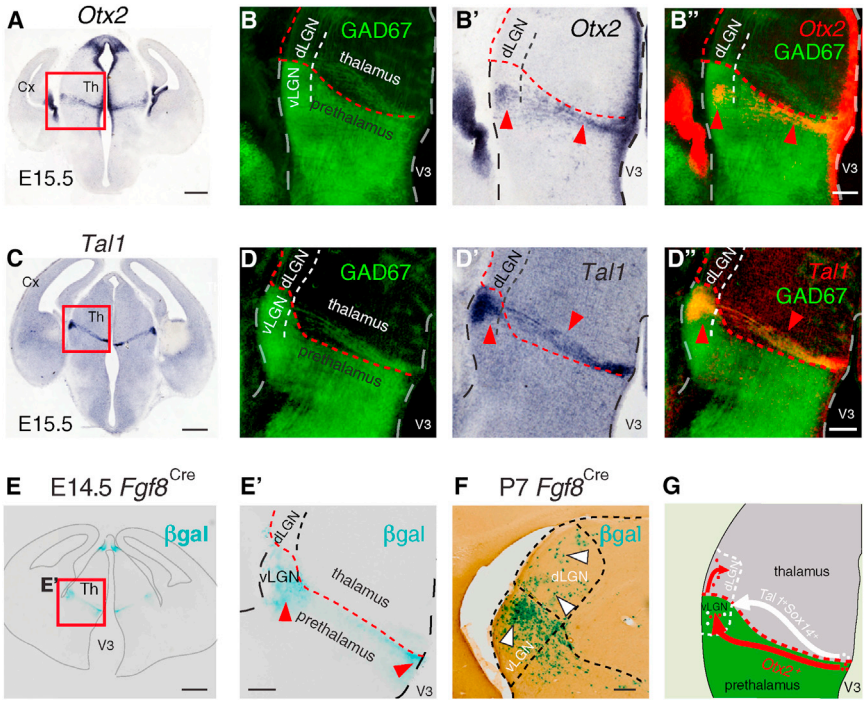

Figure 2. dLGN INs Migrate from the vLGN and Are Born from a Prethalamic Progenitor Microdomain

(A–B″) At E15.5, *Otx2*$^+$ INs (A; red arrowheads in B′ and B″) form a ventral stream of cells in the prethalamus, bridging a microdomain on the V3 wall with the ventral vLGN.

(C–D″) *Tal1*$^+$ *Otx2*$^-$ INs (C; red arrowheads in D′ and D″) take a distinct, more dorsal path in the thalamus to reach the dorsal vLGN. (B″) and (D″) are overlays of (B) and (B′) and (D) and (D′), respectively, with the ISH pseudocolored in red. Dashed red line indicates borders of the thalamus proper.

(E–F) Genetic fate mapping in *Fgf8*^{Cre}/βgal^{STOPflox} transgenic mice specifically labels neurons in the ventral stream (E; red arrowheads in E′) at E14.5 and INs in the vLGN and dLGN at P7 (white arrowheads in F).

(G) Schematic summary of the findings. Scale bars represent 300 μm in (A), (C), and (E); 100 μm in (B)–(B″), (D)–(D″), and (E′); and 50 μm in (F). Abbreviations: Cx, cortex; Th, thalamus; V3, third ventricle. See also Figure S2.

and radial migration of dLGN INs. This abnormal "laminar" distribution reflected abnormal migration rather than selective cell death, since the total number of dLGN INs and expression of the apoptotic marker cleaved caspase-3 were unaffected by ONS (Figure 4H–4I′; Ctl: 250 ± 14 GFP$^+$ INs/section; ONS 262 ± 10 GFP$^+$ INs/section; p = 0.5, n = 1,167 Ctl INs, n = 1,219 ONS INs, Student's t test). Confirming these findings, IN migration was also impaired in *Ey1* anophthalmic mice, which have a specific defect in eye formation during embryogenesis (Tucker et al., 2001; Charbonneau et al., 2012) (Figures 4J–4N). Together, these findings indicate that retinal input is required for the laminar positioning of INs within the dLGN.

We next examined whether retinal input was also required at a later stage of dLGN IN differentiation, i.e., during synaptogenesis. For this purpose, we took advantage of the dLGN IN-specific pre- and postsynaptic markers *Cplx3* and *α6 nAChR* identified above (Figures 1I–1R″). Eliminating retinal input at birth by ONS or prenatally in *Ey1* mice induced a dramatic repression of the transcripts for the presynaptic protein *Cplx3* and the vesicular transporter for GABA, VGAT. The *α6* subunit of the postsynaptic nicotinic cholinergic receptor (*α6 nAChR*) was also repressed, leading to specific loss of cholinergic responses in dLGN INs but not TC neurons (Figures 5A–5F, quantified in 5M–5O, and S4A–S4H). In contrast, *Otx2* expression was only minimally changed, and expression of other IN-specific genes such as GABA, Reelin, and the β3 subunit of postsynaptic nicotinic cholinergic receptor was unaffected (Figures S4I–S4K and data not shown), indicating that retinal input controls specific genetic differentiation programs in dLGN INs.

To distinguish whether this abnormal molecular synaptic differentiation was the consequence of IN mismigration or was independently regulated by retinal input, we performed an ONS at P8, after completion of neuronal migration (Figure 1D). Supporting an independent regulation of synaptic differentiation by retinal input, we found that the synaptic markers *Cplx3* and *α6 nAChR* were strongly downregulated after P8 ONS, despite the normal distribution of INs within the dLGN (Figures 5G–5I). Interestingly, *Otx2* expression was unaffected, consistent with a primary role of this transcription factor in migration rather than synaptogenesis. In contrast, inhibition of neuronal firing by overexpression of the voltage-gated potassium channel Kir2.1 (De Marco García et al., 2011) into dLGN INs repressed *Cplx3* expression without detectably affecting migration (Figures S4L and S4M″; Ctl: 82/82 Cplx3$^+$ INs [Figure 1N″], Kir2.1: 3/23 Cplx3$^+$ INs, n = 2 mice, p < 0.0001, Fisher's exact test). This further suggests that migration and synaptogenesis are differentially regulated and supports a requirement for cell-intrinsic neuronal activity in dLGN IN synapse formation, as previously reported for select neocortical IN subtypes (De Marco García et al., 2011). Finally, ONS at P12 did not affect molecular synaptic differentiation (Figures 5J–5L), thereby defining the end of a "critical period" for input-dependent synaptic differentiation of dLGN INs.

Impaired Migration and Synaptic Differentiation of INs Leads to Disinhibition of TC Neurons

We next examined whether abnormal migration (P0–P8) and/or synaptic differentiation (P8–P12) of dLGN INs following ONS results in increased excitability of postsynaptic dLGN TC neurons (Figures 6A and 6B). We determined excitability by counting the number of action potentials in ~P20 TC neurons in response to brief current pulses in slices from mice that underwent ONS at P1, P8, or P12 (Figures 6B and 6C). TC neuron excitability was dramatically increased following P1 and P8 ONS but normal after P12 ONS (Figure 6C), suggesting that TC excitability increases when IN migration or synaptic differentiation is impaired.

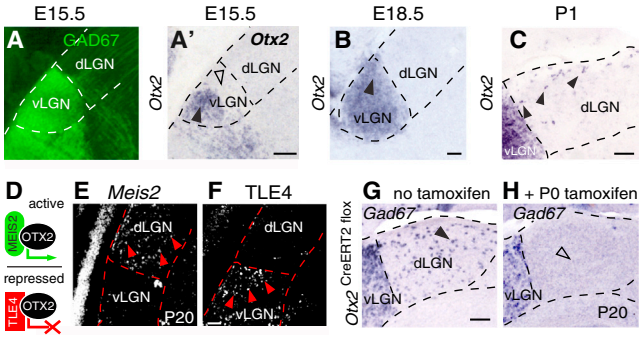

Figure 3. dLGN INs Require *Otx2* Function Postnatally

(A) Coronal section from an E15.5 GAD67^{GFP} brain showing delineation between the vLGN, which is rich in INs, and the dLGN, which is devoid of these neurons.

(A′–C) At E15.5, *Otx2*$^{+}$ INs are located in the ventral part of the vLGN (A′, same slice as A) and progressively migrate toward the vLGN-dLGN border (E18.5; B) before entering into the dLGN at P1 (C, arrowheads).

(D) MEIS2 is an OTX2 activator, while TLE4 is an OTX2 repressor.

(E and F) *Meis2* is expressed by dLGN INs but not by vLGN INs (E, arrowheads), while TLE4 has a complementary pattern of expression (F, arrowheads).

(G and H) Loss of OTX2 function in *Otx2*$^{+}$ INs (arrowhead in G) by P0 injection of tamoxifen in *Otx2*^{CreERT2}/*Otx2*^{flox} mice leads to a specific loss of INs in the dLGN (empty arrowhead in H). Scale bars represent 100 μm. See also Figure S3.

To demonstrate the involvement of dLGN INs in controlling TC neuron excitability, we next pharmacologically activated IN presynaptic terminals with the metabotropic glutamate receptor group I (mGluR-I) agonist. In agreement with previous studies, DHPG evoked inhibitory responses in TC neurons (Figure 6D; Cox and Sherman, 2000; Errington et al., 2011; Govindaiah and Cox, 2006). In contrast, these responses were not evoked following P1 or P8 ONS but were still present following P12 ONS, identifying a critical period for TC neuron inhibition by dLGN INs (Figure 6D). Direct stimulation of IN-TC synapses using optogenetic activation of channelrhodopsin-2 (ChR2)-expressing dLGN INs (see Experimental Procedures) further confirmed reduced inhibitory input onto TC neurons following P1 ONS (Figure 6E).

Finally, we directly examined whether lack of dLGN INs leads to hyperexcitability of TC neurons. For this purpose, we took advantage of the *Otx2*^{CreERT2}/*Otx2*^{flox} transgenic mice described above, in which dLGN INs are specifically eliminated by P0 tamoxifen injection (see Figures 3G and 3H). In contrast to noninjected controls, which displayed normal input-output responses, TC neuron excitability was increased in tamoxifen-injected transgenic mice (Figure 6F), directly demonstrating a causal link between decreased inhibition and TC neuron hyperexcitability. Taken together, these data indicate that retinal input is required for the functional integration of dLGN INs, thus controlling the excitability of TC circuits.

Retinal Waves Direct the Migration and Synaptic Integration of dLGN INs

Although both microsurgical and genetic ablation of the eye reveal that retinal input is necessary for dLGN IN migration and synaptic differentiation, whether specific patterns of retinal activity are required for these inhibitory circuits to form remains unaddressed.

In mice, eyes do not open before P15; accordingly, dark rearing from birth did not affect dLGN IN migration or synaptic differentiation (Figure S5A). During the first postnatal week, however, "retinal waves" (Meister et al., 1991), rather than light-evoked activity, are the main source of retinogeniculate activity. These coordinated depolarizations of retinal ganglion cells are critical to the eye-specific segregation of retinogeniculate and TC axons (Penn et al., 1998; Huberman et al., 2008; Stafford et al., 2009; Ackman et al., 2012), but whether they are also required for inhibitory circuit assembly is unknown. To investigate this possibility, we took advantage of *Chrnb2*$^{-/-}$ mice, a whole-body knockout line in which stage 2 retinal waves are abolished during the first postnatal week (Bansal et al., 2000; Muir-Robinson et al., 2002; McLaughlin et al., 2003; Sun et al., 2008; Stafford et al., 2009). Supporting a critical role for retinal waves in the assembly of dLGN inhibitory circuits, the distribution of INs was abnormal in GAD67^{GFP}-*Chrnb2*$^{-/-}$ mice. INs, which do not express *Chrnb2* (Figure S5B), were predominantly located in the superficial half of this nucleus (Figures 7A–7E, S5C, and S5D), similar to what was observed after optic nerve section. Loss of retinal waves also affected the synaptic integration of dLGN INs, as indicated by a dramatic repression of the transcripts for the presynaptic proteins *Cplx3* and VGAT, and the postsynaptic protein *α6 nAChR* (Figures 7F, 7G, S5E, and S5F). IN mismigration and synaptic misdifferentiation could also be elicited by daily P0–P10 intraocular injections of epibatidine, a high-affinity cholinergic agonist that blocks retinal waves in vitro and in vivo (Ackman et al., 2012) (Figures S5G–S5O). Interestingly, dLGN IN migration was less disrupted by perturbation of retinal waves than by physical loss of retinal input (i.e., ONS and *Ey1* mice) (Figure S5P), suggesting that retinal wave-independent mechanisms contribute to the migration of INs within the dLGN. Finally, consistent with abnormal functional assembly of dLGN inhibitory circuits, TC neuron excitability was dramatically increased in *Chrnb2*$^{-/-}$ mice, while DHPG-evoked inhibitory responses were strongly reduced (Figures 7H and 7I). Taken together, these results indicate that retinal waves are required during the first postnatal week for the assembly of dLGN inhibitory circuits.

DISCUSSION

The two main findings of this study are that INs of the visual thalamus are recruited into retinogeniculate circuits from the vLGN, an evolutionarily older retinal target, and that the laminar and synaptic integration of these INs into visual circuits is controlled by patterns of retinal activity. These findings reveal an input-dependent mechanism for circuit construction in the CNS, in which the level and pattern of activity within a target circuit controls the incorporation of migrating inhibitory neurons. Such use-dependent homeostatic recruitment is well suited to balance excitatory and inhibitory activity during development and may have driven the experience-dependent incorporation of inhibitory units into increasingly complex excitatory circuits during vertebrate evolution.

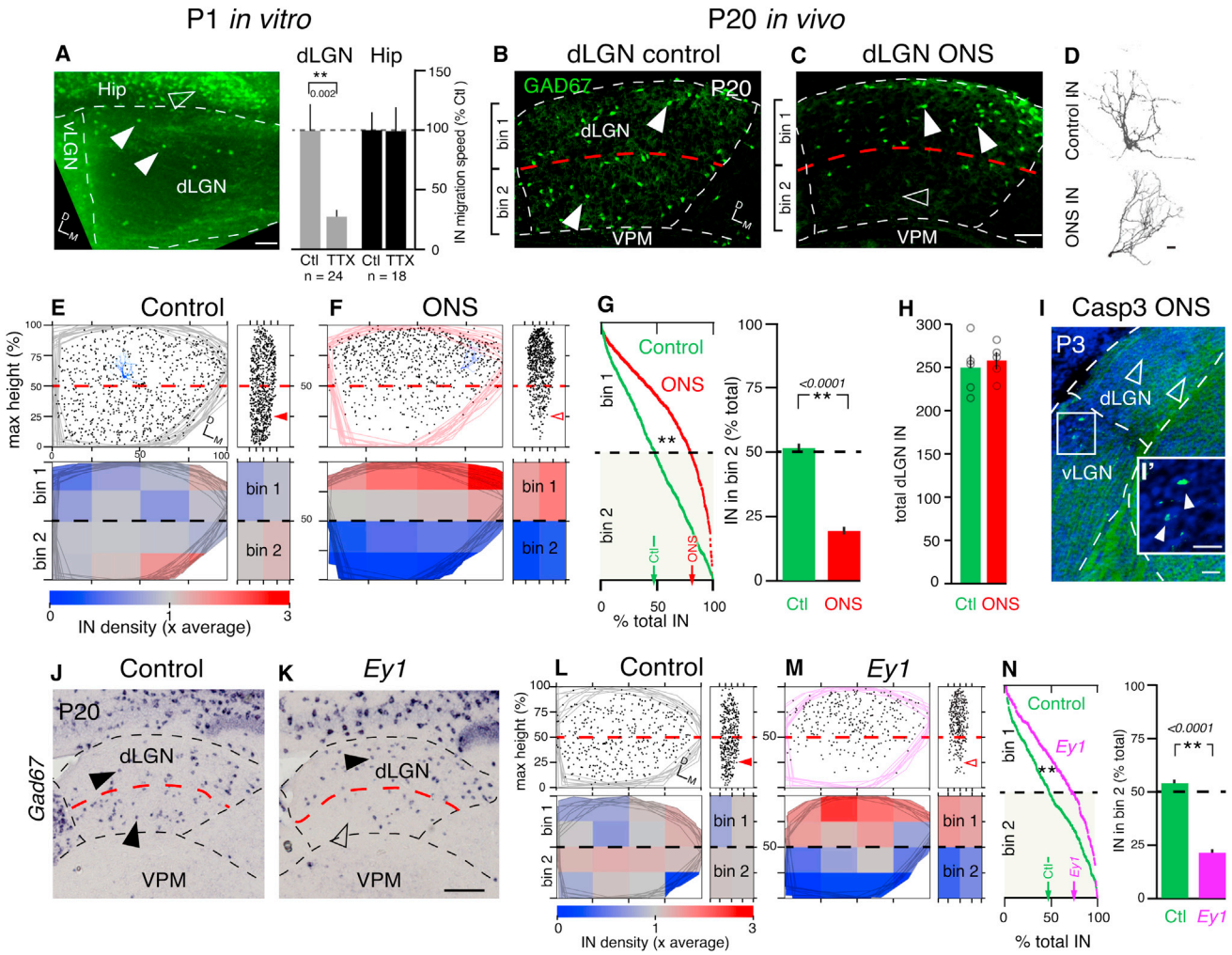

Figure 4. Retinal Input Directs the Migration of dLGN INs

(A) Time-lapse image of the dLGN in GAD67^{GFP} mice at P1. Individual INs are visible in the dLGN (white arrowheads) and hippocampus (empty arrowhead). Application of TTX specifically affects the migration of dLGN INs, while hippocampal INs are unaffected. Paired t test.

(B–D) P1 optic nerve section (ONS) causes abnormal distribution of dLGN INs (arrowheads in B), which remain at more superficial locations than in control littermates (arrowheads in C), where they morphologically differentiate (biocytin labeling in D). Dashed red line indicates separation between bin 1 (superficial) and 2 (deep).

(E–G) Summary of the results. (E and F) Top: cumulative scatter plot showing location of individual INs in control (E) and ONS (F) mice. Outlines of the dLGN are indicated in gray and normalized for maximum width and height. The location of the neurons shown in (D) is indicated. The same scatter plot is shown on the right with x axis scaled down to highlight lack of INs at deep locations (red arrowheads). Bottom: IN density heatmap (left, 4 × 4 grid; right, 2 × 2 grid), showing accumulation of INs at superficial locations after ONS. (G) Quantification of the data shown in (E) and (F) using cumulative distribution (left) and fraction of bin 2-located INs (right). n = 1,167 Ctl INs, n = 1,219 ONS INs, 5 mice per condition. Cumulative distribution: **p < 0.0001, Kolmogorov-Smirnov test. Bin 2 fraction: Fisher's exact test.

(H–I′) ONS does not lead to IN cell death, as indicated by total counts of INs (H) and absence of cleaved Casp3^{+} neurons in the dLGN (I and I′).

(J and K) dLGN INs fail to migrate to deeper tiers of the dLGN in *Ey1* anophthalmic mice (K) compared to control mice (J).

(L–N) Cumulative scatter plots (L and M, see E and F for details) and quantifications (N) show accumulation of INs in bin 1. n = 413 Ctl INs, n = 315 ONS INs, 3 mice per condition. Cumulative distribution: **p < 0.0001, Kolmogorov-Smirnov test. Bin 2 fraction: Fisher's exact test. Abbreviations: Ctl, control; Hip, hippocampus; ONS, optic nerve section; TTX, tetrodotoxin. Scale bars represent 100 μm in (A)–(C), (I)–(K); 10 μm in (D); and 50 μm (I) and (I′). Values are represented as mean ± SEM.

Regulation of Circuit Homeostasis by Modulation of Inhibition

Inhibitory input is central to homeostatic synaptic plasticity in the adult somatosensory and visual cortices, where decreases in circuit activity after visual deprivation (Maffei et al., 2004), or increases after whisker stimulation (Knott et al., 2002), lead to compensatory changes in inhibitory synapses (Pozo and Goda, 2010; Wenner, 2011). Similarly, circuit activity can regulate the synthesis of inhibitory neurotransmitters: during spinal cord and tectum development in *Xenopus laevi*, synthesis of GABA

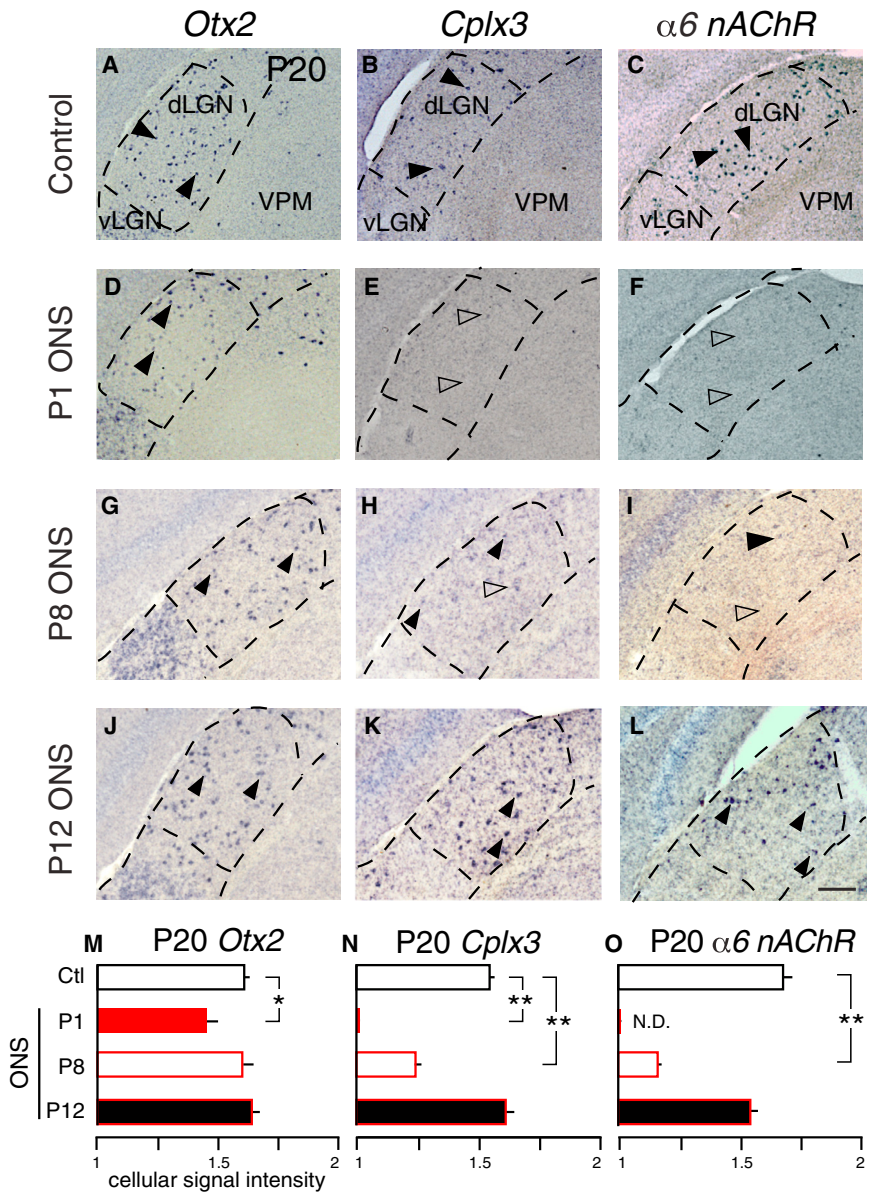

Figure 5. Retinal Input Directs the Synaptic Differentiation of dLGN INs during a Critical Period of Development

(A–F) The synaptic differentiation of dLGN INs is impaired by P1 ONS: compared to control mice (A–C), *Otx2* expression is mildly decreased by P20 (D), while *Cplx3* (E) and *α6 nAChR* (F) are fully repressed after ONS.

(G–L) When ONS is performed at P8 (G–I), there are no migratory abnormalities (G), but the expression of the synaptic proteins *Cplx3* (H) and *α6 nAChR* (I) is strongly decreased, which is not the case when ONS is performed at P12 (J–L).

(M–O) Quantification of expression illustrated in (A)–(L); a signal intensity of 1 corresponds to background levels. *p = 0.01, **p < 0.005, Student's t test, n ≥ 39 INs per condition. Abbreviation: ND, not detectable. Scale bar represents 100 μm. Values are represented as mean ± SEM. See also Figure S4.

changes with circuit activity (Borodinsky et al., 2004; Miraucourt et al., 2012) and, in adult primates, visual deprivation reversibly decreases GABA expression in the visual cortex (Hendry and Jones, 1986, 1988). To the best of our knowledge, our findings provide the first instance in which circuit homeostasis is achieved by regulating the incorporation of migrating inhibitory neurons during development.

Inhibitory Neurons Are Recruited into dLGN Visual Circuits from the vLGN, an Evolutionarily Older Retinal Target

Our findings indicate that dLGN INs belong to a specialized lineage of neurons, which are born during midembryogenesis from a restricted prethalamic *Fgf8*$^{+}$ progenitor domain. These INs reside in the vLGN until birth, become molecularly distinct from neighboring INs, and progressively incorporate retinogeniculate circuits during the first postnatal week. The vLGN is an evolutionary ancient retinal target already present in fish, reptiles, and birds, which projects to the suprachiasmatic nucleus of the hypothalamus and is involved in nonimage-forming tasks such as generation of circadian rhythms (Harrington, 1997; Delogu et al., 2012). In contrast, the functional importance of the dLGN has progressively increased with expansion of retinogeniculate connections, culminating in primates (Butler, 2008; Mueller, 2012). Interestingly, the proportion of dLGN INs increases in parallel with the evolutionary development of retinogeniculate connections (Arcelli et al., 1997), with extensive IN incorporation in the dLGN of mammals with color vision and broad binocular fields. In these species, the dLGN itself dramatically expands and becomes "corticalized," i.e., has distinct layers and a variety of IN subtypes, which in humans, but not in nonhuman primates, also originate from subpallial sources (Letinic and Rakic, 2001).

Integrating our data with these findings, we propose that the increasing importance of vision in behavior and underlying expansion of retinogeniculate circuits may have driven the use-dependent recruitment of INs into the dLGN. Supporting a broader use of such a circuit construction strategy, INs progressively populate all thalamic nuclei in higher mammals, in line with the increasing complexity and expansion of TC circuits (Arcelli et al., 1997). Interestingly, *Cplx3*, *Otx2*, and Reelin are also expressed by subsets of dLGN neurons in the small New World monkey *Callithrix jacchus* (Mashiko et al., 2012; data not shown), suggesting that at least some of the dLGN IN-specific developmental programs identified here are conserved in primates.

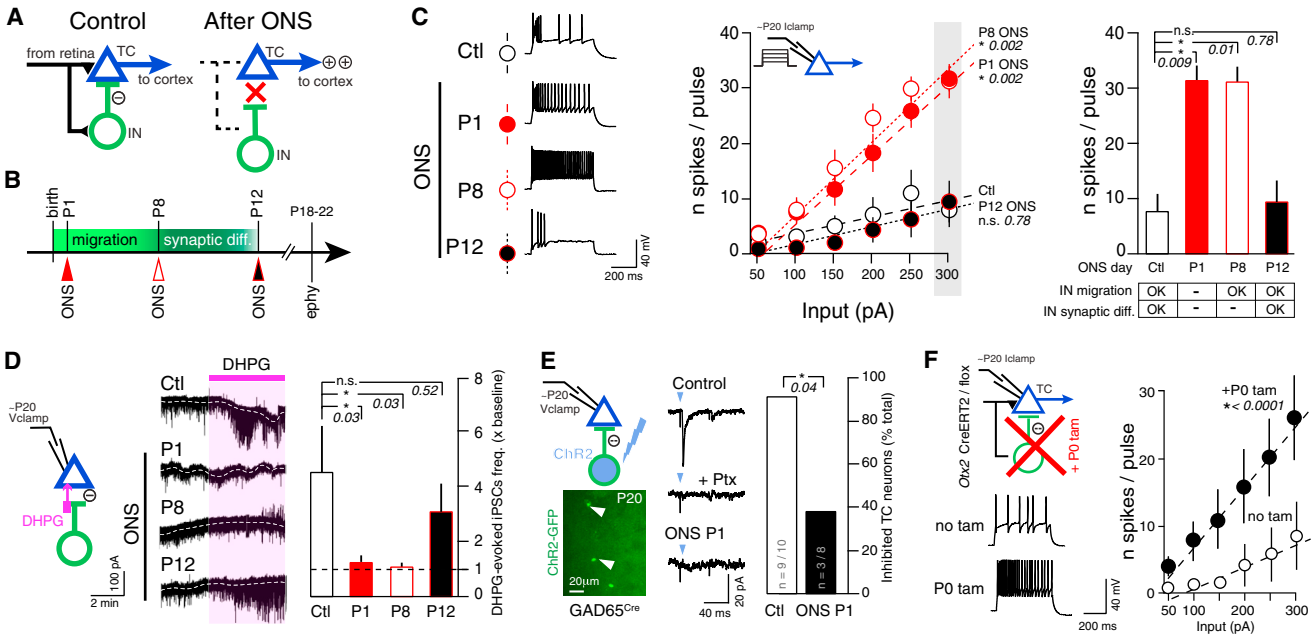

Figure 6. Impaired Migration and Synaptic Differentiation of INs Leads to Disinhibition of TC Neurons

(A) Schematic representation of the findings: decreased inhibitory input following ONS leads to hyperexcitability of TC neurons.

(B) Schematic summary of the experiments performed in (C) and (D).

(C) Perturbing IN migration (P1 ONS) or IN synaptic differentiation (P8 ONS) leads to hyperexcitability of TC neurons, while ONS at P12 (i.e., after synaptic differentiation) has no effect on excitability. Left: sample traces showing responses to a 300 pA current pulse. Middle: spike numbers in response to increasing current steps. Right: quantification of the response to a 300 pA pulse. Ctl: n = 6, P1 ONS: n = 6, P8 ONS: n = 5, P12 ONS: n = 5. Slope regression comparison with Ctl (middle), Mann-Whitney test (right).

(D) Activation of group I mGluRs by DHPG evokes strong inhibitory responses in TC neurons in control conditions that are not evoked after P1 or P8 ONS but still present following P12 ONS. Mann-Whitney test, Ctl: n = 5, P1 ONS: n = 5, P8 ONS: n = 5, P12 ONS: n = 8.

(E). Optogenetic stimulation of dLGN INs evokes picrotoxin-sensitive inhibitory responses in most TC neurons, but not following P1 ONS (Fisher's exact test). Photomicrograph shows ChR2^{+} INs in an acute 300-µm-thick GAD65^{Cre} section.

(F) TC neurons are hyperexcitable following induced ablation of INs by tamoxifen administration in Otx2$^{CRE\text{-}ERT2}$/*Otx2*^{flox} mice (see Figures 3G and 3H). No tam: n = 6, tam: n = 8. Slope regression comparison. Abbreviations: n.s., not significant; ephy, electrophysiological assessment; Ptx, picrotoxin; tam, tamoxifen. Values are represented as mean ± SEM.

Mechanisms of Circuit Integration and Implications for Visual Plasticity

While the migration of INs from the vLGN into the dLGN is independent of retinal input, appropriate laminar positioning (i.e., superficial versus deep location) of these INs requires retinogeniculate activity. This is reminiscent of the laminar migratory abnormalities found in specific subtypes of cortical INs when cell-intrinsic electrical activity is blocked, suggesting convergent mechanisms of action (De Marco García et al., 2011). Our *Otx2* loss-of-function experiments suggest a permissive role for OTX2 activation in dLGN IN differentiation or migration; supporting the latter function, this transcription factor has recently been shown to enhance neuronal migration in the hindbrain (Wortham et al., 2012).

We identify a critical period before P12 during which retinal input controls the migration (P0–P8) and synaptic differentiation (P8–P12) of dLGN INs, and our observations in *Chrnb2*$^{-/-}$ mice, in which loss of retinal waves is limited to the first postnatal week (Bansal et al., 2000; Muir-Robinson et al., 2002; McLaughlin et al., 2003), reveal a critical role for cholinergic retinal waves in setting the excitatory/inhibitory balance of dLGN circuits. Because the *Chrnb2* mutation is nonconditional, the respective contributions of retinogeniculate and TC neuron function cannot, however, fully be distinguished. Although retinotopic refinement defects reported in *Chrnb2*$^{-/-}$ mice are largely thought to be of retinal origin (see e.g., McLaughlin et al., 2003; Triplett et al., 2009), and pharmacological blockade of β2-containing nicotinic receptors did not increase TC neuron excitability in vitro (data not shown), loss of *Chrnb2* function in TC neurons may have also contributed to abnormal assembly of inhibitory circuits, perhaps via changes in their firing properties.

Nonsynaptic activation of glutamatergic receptors controls developmental neuron migration in the hippocampus and cerebellum (Komuro and Rakic, 1993; Manent et al., 2005, 2006). Therefore, activity-dependent release of glutamate may directly act to regulate IN migration within the dLGN; supporting this possibility, extracellular glutamate is reduced in the dLGN after optic nerve section (Sakurai and Okada, 1992). Similarly, synchronous depolarization of retinal ganglion cells during retinal waves probably increases extracellular glutamate levels in the dLGN and could thereby provide an instructive signal for migration by transiently activating low-affinity glutamate receptors on migrating INs.

dLGN INs may contribute to retinogeniculate and thalamocortical mapping of visual input during development, since abnormal

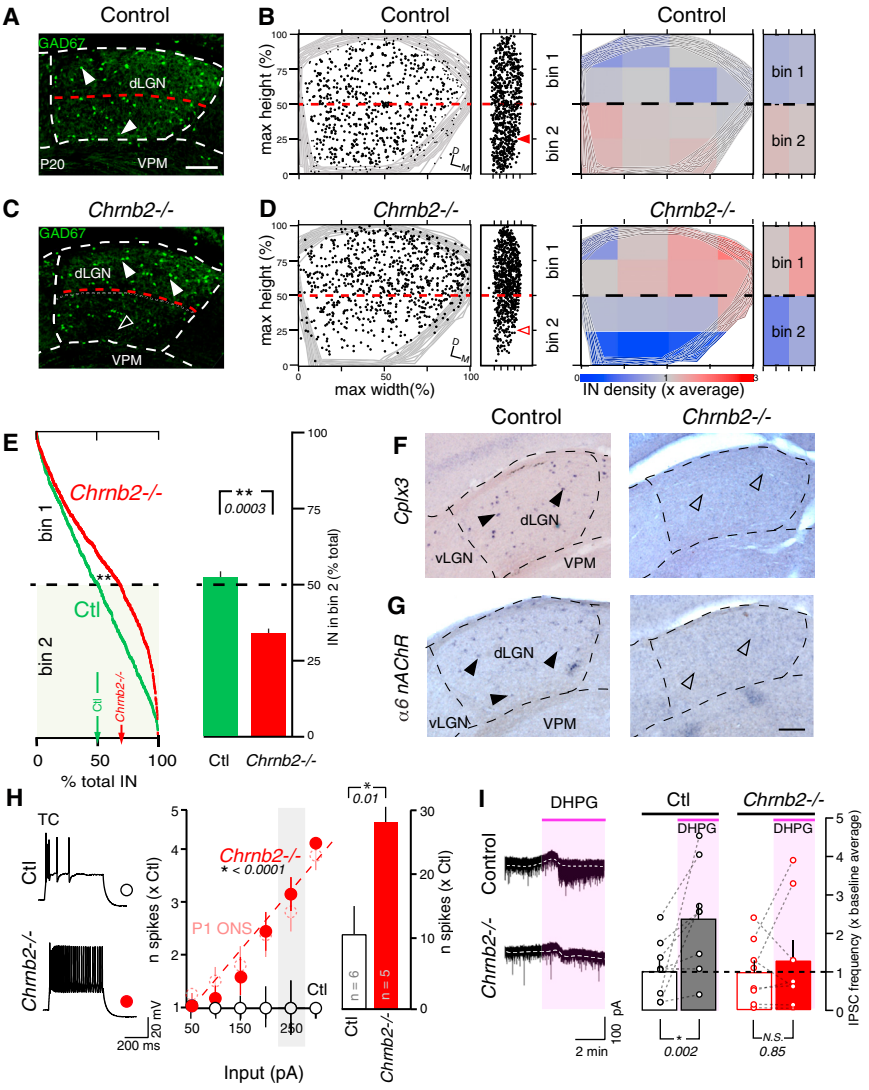

Figure 7. Retinal Waves Direct the Migration and Synaptic Integration of dLGN INs

(A–D) Loss of retinal waves in *Chrnb2*$^{-/-}$ mice causes abnormal distribution of dLGN INs, which remain at more superficial locations than in control littermates. (A and C) Photomicrographs of IN distribution in GAD67^{GFP} (A) and *Chrnb2*$^{-/-}$ -GAD67^{GFP} (C) mice. (B and D) Left: cumulative scatter plot showing location of individual INs in control (B) and *Chrnb2*$^{-/-}$ (D) mice. Right: IN density heatmap showing accumulation of INs at superficial locations in *Chrnb2*$^{-/-}$. See Figure 4 for details.

(E) Quantification of the data shown in (B) and (D) using cumulative distribution (left) and fraction of bin 2-located INs (right). n = 790 Ctl INs, n = 993 *Chrnb2*$^{-/-}$, 5 mice per condition. Cumulative distribution: **p < 0.0001, Kolmogorov-Smirnov test. Bin 2 fraction: Fisher's exact test.

(F and G) The synaptic differentiation of dLGN INs in *Chrnb2*$^{-/-}$ mice is impaired, as shown by repressed expression *Cplx3* (F) and *α6 nAChR* (G).

(H) TC neurons are hyperexcitable in *Chrnb2*$^{-/-}$ mice, as found following P1 ONS (dashed red circles, see Figure 6C). Graph on the right represents response to a 250 pA pulse, illustrated by the sample traces on the left. Slope regression comparison (middle) and Mann-Whitney test (right) are shown.

(I) DHPG fails to evoke IPSCs in TC neurons in *Chrnb2*$^{-/-}$ mice. Paired t test. Scale bars represent 100 μm in (A), (C), (F), and (G). Values are represented as mean ± SEM. See also Figure S5.

migration and synaptic integration of these neurons leads to disinhibition of TC neurons. Recent reports have established the instructive role of retinal activity in the retinotopic mapping and interocular competition of retinogeniculate axons (Zhang et al., 2012; Xu et al., 2011) and the role of activity in the maturation of cortical INs (Di Cristo et al., 2007; De Marco García et al., 2011). It will be interesting to examine whether imbalances in the eye-specific incorporation of INs contributes to the outcome of interocular competition. More broadly, it will be important to assess whether activity-driven circuit integration of INs occurs in other brain regions, e.g., via oscillatory activity such as cortical waves, and whether distinct neuronal circuits within a given area can compete to integrate specific subtypes of incoming neurons.

EXPERIMENTAL PROCEDURES

Animals

All experimental procedures were approved by the Geneva Cantonal Veterinary Authority. Embryonic day (E) 0.5 was established as the day of vaginal plug. C57/Bl6 mice were provided by Charles River Laboratories. GAD67^{GFP} mice were generated by Tamamaki and colleagues (Tamamaki et al., 2003), *Fgf8*^{Cre} mice by Toyoda and colleagues (Toyoda et al., 2010), *Chrnb2* knockout mice were obtained from Marla Feller, and *Otx2*^{CreERT2} and *Otx2*^{flox} mice were generated by Fossat and colleagues (Fossat et al., 2006). Transgenic mice were compared to littermate controls. GAD67^{GFP} knockin mice were bred as heterozygotes.

In Situ Hybridization and Image Acquisition

Tissue Collection

Mice were perfused with 0.9% NaCl followed by 4% paraformaldehyde. Brains were removed and postfixed overnight in 4% PFA at 4°C and cut at 50 μm on a vibrating microtome.

ISH

In situ hybridization on slides was performed according to methods described previously (De la Rossa et al., 2013). Briefly, hybridization was carried out overnight at 60°C with DIG-labeled RNA probes (Table S1). Following hybridization, sections were washed and incubated with alkaline phosphatase-conjugated antidigoxigenin antibody (Roche 1:2,000) overnight at 4°C. Sections were then washed and the color reaction was carried out overnight at 4°C in an NBT/BCIP solution (Roche). After color revelation, sections were washed, postfixed for 30 min in 4% PFA, and mounted with Fluoromount (Sigma).

Image Acquisition and Quantification

Photomicrographs were taken with an Eclipse 90i (Nikon) fluorescence microscope or a Zeiss LSM700 confocal microscope. For quantification of IN distribution, the dLGN was divided into two bins by tracing a curved line midway between the pial surface and dLGN-VPM boundary. Five to eight

sequential rostrocaudal sections (Paxinos atlas coordinates from Bregma: between −1.94 and −2.70) were used for quantification of distribution in control, ONS, *Ey1*, *Chrnb2*$^{-/-}$, and epibatidine/vehicle-injected mice. We observed a homogenous ∼10% decrease in the dorsoventral (12%) and lateromedial (9%) size of the dLGN following ONS. LGN size was adjusted to maximal length and height for IN scatterplots and density heatmaps across sections (Krahe et al., 2011). Quantification of ISH intensity was performed blindly using the "equalize" function of Adobe Photoshop CS6 to normalize background intensity and measuring the threshold at which ∼50% of the pixels in individual labeled neurons were visible.

Tissue Microdissection and Microarray

Pups collected from a single litter were used for each of three biological replicates of VPM and dLGN samples at P0, P3, and P10. Fresh coronal brain sections (140 μm) were cut on a vibrating microtome and VPM and dLGN nuclei were visually identified and microdissected in ice-cold oxygenated artificial cerebrospinal fluid under RNase-free conditions. Samples were stored in RNA*later* at −80°C. RNA was extracted using the Ambion *mir*Vana Isolation kit followed by two-cycle amplification and labeling was performed using MEGAscript T7 kit and MessageAmpIIaRNA amplification kit from Ambion. Labeled cRNA was applied to Affymetrix 430 2.0 mouse microarray chips. Microarray CEL files were normalized with MAS5 Affymetrix algorithm and Robust Multichip Analysis (RMA) Identification of transcripts that covaried with GAD67 was performed using the Principal Components Analysis tool of the Partek Genomics Suite software. Candidate genes were secondarily screened using the online expression databases Allen Brain Atlas and BGEM.

Surgical Procedures

Injection of a reporter plasmid under the control of Ubiquitin promoter with a fluorochrome reporter (red, Tomato) (1.6 μg/μl) or Kir 2.1 (2.0 μg/μl) (Mire et al., 2012) into the third ventricle of E12.5 timed pregnant C57/BL6 dams was performed under ultrasound guidance, and brief voltage pulses (50 mV, 50 ms) were applied using external paddles as described previously (De la Rossa et al., 2013). Pups were collected at P7. Optic nerve section (ONS) was carried out on P1 pups; animals were deeply anesthetized on ice. A small incision was made in the eyelid with a scalpel and the eye was separated from the optic nerve with scissors and removed from the orbit with forceps. Pups were briefly warmed on a heating pad and were returned to their mother. The optic tract was labeled by intravitreal injection of 1 μl of cholera toxin subunit B (0.2%) (Invitrogen) at P18 and brains were collected 48 hr later. Tamoxifen (Sigma, stocked at 20 mg/ml in corn oil,) was injected intraperitoneally at P0 (0.2 mg stock solution/g of body weight).

In Vitro Time-Lapse Imaging

P1 coronal sections (200 μm thick) from GAD67^{GFP} mice were cut on a vibrating microtome and placed in neurobasal medium (Invitrogen) supplemented with 2% B27 (GIBCO, Invitrogen), 2 mM glutamine, 1 mM sodium pyruvate, 2 mM N-acetyl-cysteine, and 1% penicillin-streptomycin. Time-lapse imaging was performed 6 hr after slice preparation for over a minimum of 20 hr in a thermoregulated chamber maintained at 37°C and at 5% CO_2. Time-lapse movies were acquired using a fluorescent microscope (Eclipse TE2000; Nikon) using a Nikon Plan 20×/0.30 objective or a Zeiss Nipkow spinning-disk confocal microscope. Images were acquired using the Open-lab software (version 5.0) every 5 min for at least 20 hr. Time-lapse stacks were generated and single-cell tracking of labeled neurons (n = 18 hippocampal INs, n = 24 dLGN INs, n = 3 mice) was performed using the Metamorph software (version 7.4). Migration speed was calculated as the total distance traveled by the cell divided by total imaging time. Values were normalized to the average migration speed of each population (hip INs and dLGN INs) in control conditions.

Electrophysiology

Coronal 300-μm-thick sections were prepared from P18–P22 mice. Slices were kept in artificial cerebrospinal fluid (30–32°C, 2–3 ml/min, submerged slices) containing 119 mM NaCl, 2.5 mM KCl, 1.3 mM MgCl, 2.5 mM $CaCl_2$, 1.0 mM Na_2HPO_4, 26.2 mM $NaHCO_3$, and 11 mM glucose bubbled with 95% O_2 and 5% CO_2. TC neurons were identified by their large round soma and their relatively hyperpolarized V_m compared to INs, as previously described (Williams et al., 1996). These criteria were confirmed in experiments in which GAD67^{GFP} mice were used and following biocytin filling of INs. Slices were visualized with a 40× objective lens. Neurons were recorded by means of whole-cell voltage clamp at −60 mV except for excitability measurements where current clamp was used. Access resistances were monitored by a hyperpolarizing step of −4 mV at the onset of every sweep and the experiment was discarded if the access resistance changed by more than 20%. The internal solution contained 140 mM K^+-gluconate, 5 mM KCl, 10 mM HEPES, 0.2 mM EGTA, 2 mM $MgCl_2$, 4 mM Na_2ATP, 0.3 mM Na_3GTP, and 10 mM creatine-phosphate except for siPSC recordings where the solution was 30 mM K-gluconate, 100 mM KCl, 4 mM Mg_2Cl_2, 10 mM creatine-phosphate, 3.4 mM Na_2ATP, 0.1 mM Na_3GTP, 1.1 mM EGTA, and 5 mM HEPES (reversal potential for Cl^-: −5 mV and K^+: −104 mV). Kynurenic acid (2 mM) was added to block glutamatergic transmission in experiments when measuring DHPG (60 μM)-evoked inhibitory postsynaptic currents (IPSCs). Currents were amplified (Multiclamp 700B, Axon Instruments), filtered at 5 kHz, and digitized at 20 kHz (National Instruments Board PCI-MIO-16E4, Igor, WaveMetrics). The liquid junction potential was not corrected. The firing patterns of individual neurons were determined by step current injections of 500 ms.

For optogenetic stimulation, stereotaxic injections of an AAV5-floxed-ChR2 virus (160 nl, Addgene, UNC Vectore Core) were performed at P6 in GAD65^{Cre} mice (Kätzel et al., 2011) into the dLGN (coordinates from Lambda: AP + 1.34 mm, ML + 2.00 mm, depth 2.60 mm), resulting in infection of ∼50% of dLGN INs. ChR2 was stimulated by flashing a 470 nm blue light (0.1–2 ms) at 0.1 Hz through the light path of the microscope (40× lens) using an LED under computer control. Recorded TC neurons were located within ∼200 μm of ChR2-expressing INs. Light-evoked IPSCs were recorded in the presence of kynurenic acid (2 mM). Picrotoxin (100 μM) was used to confirm the GABAergic nature of the photo-evoked currents.

For cell filling, dLGN INs were visually identified in GAD67^{GFP} mice and filled with 3 mg/ml biocytin for at least 30 min. Sections were fixed for 2 hr and biocytin immunocytochemistry was performed using a streptavidin-conjugated Cy3 antibody (Jackson ImmunoResearch).

SUPPLEMENTAL INFORMATION

Supplemental Information includes Supplemental Experimental Procedures and five figures and can be found with this article online at http://dx.doi.org/10.1016/j.neuron.2014.01.032.

AUTHOR CONTRIBUTIONS

G.P. and C.B. contributed equally to this work.

ACKNOWLEDGMENTS

We are thankful to Florian Smets and Audrey Benoit for technical assistance and to the members of our laboratories and Eiman Azim for helpful comments and contributing to improve the manuscript. We thank Dr. T. Lamonerie for the gift of *Otx2* Cre^{ERT2} and*Otx2*^{flox} mice, Dr. M. Feller for providing *Chrnb2*$^{-/-}$ brains and mice, Dr. D. Boire for providing the *Ey1* brains, and Dr. G. Lopez-Bendito for providing the Kir2.1-GFP construct. C.B. is supported by an Ambizione grant from the Swiss National Science Foundation; C.L. is supported by the Swiss National Science Foundation; A.D. is supported by the Swiss National Science Foundation and the NCCR Synapsy; work in the Jabaudon laboratory is supported by the Swiss National Science Foundation, the Velux Foundation, the Leenaards Foundation, and the NARSAD Foundation.

Accepted: January 13, 2014
Published: March 5, 2014

REFERENCES

Ackman, J.B., Burbridge, T.J., and Crair, M.C. (2012). Retinal waves coordinate patterned activity throughout the developing visual system. Nature *490*, 219–225.

Agoston, Z., and Schulte, D. (2009). Meis2 competes with the Groucho co-repressor Tle4 for binding to Otx2 and specifies tectal fate without induction of a secondary midbrain-hindbrain boundary organizer. Development *136*, 3311–3322.

Akerman, C.J., and Cline, H.T. (2007). Refining the roles of GABAergic signaling during neural circuit formation. Trends Neurosci. *30*, 382–389.

Arcelli, P., Frassoni, C., Regondi, M.C., De Biasi, S., and Spreafico, R. (1997). GABAergic neurons in mammalian thalamus: a marker of thalamic complexity? Brain Res. Bull. *42*, 27–37.

Bansal, A., Singer, J.H., Hwang, B.J., Xu, W., Beaudet, A., and Feller, M.B. (2000). Mice lacking specific nicotinic acetylcholine receptor subunits exhibit dramatically altered spontaneous activity patterns and reveal a limited role for retinal waves in forming ON and OFF circuits in the inner retina. J. Neurosci. *20*, 7672–7681.

Berardi, N., and Morrone, M.C. (1984). The role of gamma-aminobutyric acid mediated inhibition in the response properties of cat lateral geniculate nucleus neurones. J. Physiol. *357*, 505–523.

Bickford, M.E., Slusarczyk, A., Dilger, E.K., Krahe, T.E., Kucuk, C., and Guido, W. (2010). Synaptic development of the mouse dorsal lateral geniculate nucleus. J. Comp. Neurol. *518*, 622–635.

Blitz, D.M., and Regehr, W.G. (2005). Timing and specificity of feed-forward inhibition within the LGN. Neuron *45*, 917–928.

Borodinsky, L.N., Root, C.M., Cronin, J.A., Sann, S.B., Gu, X., and Spitzer, N.C. (2004). Activity-dependent homeostatic specification of transmitter expression in embryonic neurons. Nature *429*, 523–530.

Bortone, D., and Polleux, F. (2009). KCC2 expression promotes the termination of cortical interneuron migration in a voltage-sensitive calcium-dependent manner. Neuron *62*, 53–71.

Butler, A.B. (2008). Evolution of the thalamus: a morphological and functional review. Thalamus Relat. Syst. *4*, 35–58.

Cajal, S.R.Y. (2002). Texture of the Nervous System of Man and the Vertebrates, Volume III. (New York: Springer-Verlag).

Charbonneau, V., Laramée, M.-E., Boucher, V., Bronchti, G., and Boire, D. (2012). Cortical and subcortical projections to primary visual cortex in anophthalmic, enucleated and sighted mice. Eur. J. Neurosci. *36*, 2949–2963.

Cox, C.L., and Sherman, S.M. (2000). Control of dendritic outputs of inhibitory interneurons in the lateral geniculate nucleus. Neuron *27*, 597–610.

De la Rossa, A., Bellone, C., Golding, B., Vitali, I., Moss, J., Toni, N., Lüscher, C., and Jabaudon, D. (2013). In vivo reprogramming of circuit connectivity in postmitotic neocortical neurons. Nat. Neurosci. *16*, 193–200.

De Marco García, N.V., Karayannis, T., and Fishell, G. (2011). Neuronal activity is required for the development of specific cortical interneuron subtypes. Nature *472*, 351–355.

Delogu, A., Sellers, K., Zagoraiou, L., Bocianowska-Zbrog, A., Mandal, S., Guimera, J., Rubenstein, J.L.R., Sugden, D., Jessell, T., and Lumsden, A. (2012). Subcortical visual shell nuclei targeted by ipRGCs develop from a $Sox14^{+}$-GABAergic progenitor and require Sox14 to regulate daily activity rhythms. Neuron *75*, 648–662.

Di Cristo, G., Chattopadhyaya, B., Kuhlman, S.J., Fu, Y., Bélanger, M.-C., Wu, C.Z., Rutishauser, U., Maffei, L., and Huang, Z.J. (2007). Activity-dependent PSA expression regulates inhibitory maturation and onset of critical period plasticity. Nat. Neurosci. *10*, 1569–1577.

Errington, A.C., Di Giovanni, G., Crunelli, V., and Cope, D.W. (2011). mGluR control of interneuron output regulates feedforward tonic GABAA inhibition in the visual thalamus. J. Neurosci. *31*, 8669–8680.

Fossat, N., Chatelain, G., Brun, G., and Lamonerie, T. (2006). Temporal and spatial delineation of mouse Otx2 functions by conditional self-knockout. EMBO Rep. *7*, 824–830.

Gelman, D.M., and Marín, O. (2010). Generation of interneuron diversity in the mouse cerebral cortex. Eur. J. Neurosci. *31*, 2136–2141.

Govindaiah, G., and Cox, C.L. (2006). Metabotropic glutamate receptors differentially regulate GABAergic inhibition in thalamus. J. Neurosci. *26*, 13443–13453.

Harrington, M.E. (1997). The ventral lateral geniculate nucleus and the intergeniculate leaflet: interrelated structures in the visual and circadian systems. Neurosci. Biobehav. Rev. *21*, 705–727.

Hayes, S.G., Murray, K.D., and Jones, E.G. (2003). Two epochs in the development of gamma-aminobutyric acidergic neurons in the ferret thalamus. J. Comp. Neurol. *463*, 45–65.

Heimbucher, T., Murko, C., Bajoghli, B., Aghaallaei, N., Huber, A., Stebegg, R., Eberhard, D., Fink, M., Simeone, A., and Czerny, T. (2007). Gbx2 and Otx2 interact with the WD40 domain of Groucho/Tle corepressors. Mol. Cell. Biol. *27*, 340–351.

Hendry, S.H., and Jones, E.G. (1986). Reduction in number of immunostained GABAergic neurones in deprived-eye dominance columns of monkey area 17. Nature *320*, 750–753.

Hendry, S.H., and Jones, E.G. (1988). Activity-dependent regulation of GABA expression in the visual cortex of adult monkeys. Neuron *1*, 701–712.

Hensch, T.K. (2005). Critical period plasticity in local cortical circuits. Nat. Rev. Neurosci. *6*, 877–888.

Hooks, B.M., and Chen, C. (2007). Critical periods in the visual system: changing views for a model of experience-dependent plasticity. Neuron *56*, 312–326.

Hu, B., Li, X., Zhou, Y., and Shou, T. (2000). Effects of bicuculline on direction-sensitive relay cells in the dorsal lateral geniculate nucleus (LGNd) of cats. Brain Res. *885*, 87–93.

Huberman, A.D., Feller, M.B., and Chapman, B. (2008). Mechanisms underlying development of visual maps and receptive fields. Annu. Rev. Neurosci. *31*, 479–509.

Isaacson, J.S., and Scanziani, M. (2011). How inhibition shapes cortical activity. Neuron *72*, 231–243.

Jeong, Y., Dolson, D.K., Waclaw, R.R., Matise, M.P., Sussel, L., Campbell, K., Kaestner, K.H., and Epstein, D.J. (2011). Spatial and temporal requirements for sonic hedgehog in the regulation of thalamic interneuron identity. Development *138*, 531–541.

Jones, E.G. (2002). Dichronous appearance and unusual origins of GABA neurons during development of the mammalian thalamus. Thalamus Relat. Syst. *1*, 283–288.

Kataoka, A., and Shimogori, T. (2008). Fgf8 controls regional identity in the developing thalamus. Development *135*, 2873–2881.

Kätzel, D., Zemelman, B.V., Buetfering, C., Wölfel, M., and Miesenböck, G. (2011). The columnar and laminar organization of inhibitory connections to neocortical excitatory cells. Nat. Neurosci. *14*, 100–107.

Knott, G.W., Quairiaux, C., Genoud, C., and Welker, E. (2002). Formation of dendritic spines with GABAergic synapses induced by whisker stimulation in adult mice. Neuron *34*, 265–273.

Komuro, H., and Rakic, P. (1993). Modulation of neuronal migration by NMDA receptors. Science *260*, 95–97.

Krahe, T.E., El-Danaf, R.N., Dilger, E.K., Henderson, S.C., and Guido, W. (2011). Morphologically distinct classes of relay cells exhibit regional preferences in the dorsal lateral geniculate nucleus of the mouse. J. Neurosci. *31*, 17437–17448.

Letinic, K., and Rakic, P. (2001). Telencephalic origin of human thalamic GABAergic neurons. Nat. Neurosci. *4*, 931–936.

Lodato, S., Rouaux, C., Quast, K.B., Jantrachotechatchawan, C., Studer, M., Hensch, T.K., and Arlotta, P. (2011). Excitatory projection neuron subtypes control the distribution of local inhibitory interneurons in the cerebral cortex. Neuron *69*, 763–779.

López-Bendito, G., and Molnár, Z. (2003). Thalamocortical development: how are we going to get there? Nat. Rev. Neurosci. *4*, 276–289.

López-Bendito, G., Sánchez-Alcañiz, J.A., Pla, R., Borrell, V., Picó, E., Valdeolmillos, M., and Marín, O. (2008). Chemokine signaling controls

intracortical migration and final distribution of GABAergic interneurons. J. Neurosci. *28*, 1613–1624.

Maffei, A., Nelson, S.B., and Turrigiano, G.G. (2004). Selective reconfiguration of layer 4 visual cortical circuitry by visual deprivation. Nat. Neurosci. *7*, 1353–1359.

Manent, J.-B., Demarque, M., Jorquera, I., Pellegrino, C., Ben-Ari, Y., Aniksztejn, L., and Represa, A. (2005). A noncanonical release of GABA and glutamate modulates neuronal migration. J. Neurosci. *25*, 4755–4765.

Manent, J.-B., Jorquera, I., Ben-Ari, Y., Aniksztejn, L., and Represa, A. (2006). Glutamate acting on AMPA but not NMDA receptors modulates the migration of hippocampal interneurons. J. Neurosci. *26*, 5901–5909.

Mashiko, H., Yoshida, A.C., Kikuchi, S.S., Niimi, K., Takahashi, E., Aruga, J., Okano, H., and Shimogori, T. (2012). Comparative anatomy of marmoset and mouse cortex from genomic expression. J. Neurosci. *32*, 5039–5053.

Meister, M., Wong, R.O., Baylor, D.A., and Shatz, C.J. (1991). Synchronous bursts of action potentials in ganglion cells of the developing mammalian retina. Science *252*, 939–943.

McLaughlin, T., Torborg, C.L., Feller, M.B., and O'Leary, D.D.M. (2003). Retinotopic map refinement requires spontaneous retinal waves during a brief critical period of development. Neuron *40*, 1147–1160.

Miraucourt, L.S., Silva, J.S., Burgos, K., Li, J., Abe, H., Ruthazer, E.S., and Cline, H.T. (2012). GABA expression and regulation by sensory experience in the developing visual system. PLoS ONE *7*, e29086.

Mire, E., Mezzera, C., Leyva-Díaz, E., Paternain, A.V., Squarzoni, P., Bluy, L., Castillo-Paterna, M., López, M.J., Peregrín, S., Tessier-Lavigne, M., et al. (2012). Spontaneous activity regulates Robo1 transcription to mediate a switch in thalamocortical axon growth. Nat. Neurosci. *15*, 1134–1143.

Miyoshi, G., and Fishell, G. (2011). GABAergic interneuron lineages selectively sort into specific cortical layers during early postnatal development. Cereb. Cortex *21*, 845–852.

Mueller, T. (2012). What is the thalamus in zebrafish? Front. Neurosci. *6*, 64.

Muir-Robinson, G., Hwang, B.J., and Feller, M.B. (2002). Retinogeniculate axons undergo eye-specific segregation in the absence of eye-specific layers. J. Neurosci. *22*, 5259–5264.

Norton, T.T., and Godwin, D.W. (1992). Inhibitory GABAergic control of visual signals at the lateral geniculate nucleus. Prog. Brain Res. *90*, 193–217.

Ortino, B., Inverardi, F., Morante-Oria, J., Fairén, A., and Frassoni, C. (2003). Substrates and routes of migration of early generated neurons in the developing rat thalamus. Eur. J. Neurosci. *18*, 323–332.

Penn, A.A., Riquelme, P.A., Feller, M.B., and Shatz, C.J. (1998). Competition in retinogeniculate patterning driven by spontaneous activity. Science *279*, 2108–2112.

Pozo, K., and Goda, Y. (2010). Unraveling mechanisms of homeostatic synaptic plasticity. Neuron *66*, 337–351.

Reim, K., Regus-Leidig, H., Ammermüller, J., El-Kordi, A., Radyushkin, K., Ehrenreich, H., Brandstätter, J.H., and Brose, N. (2009). Aberrant function and structure of retinal ribbon synapses in the absence of complexin 3 and complexin 4. J. Cell Sci. *122*, 1352–1361.

Runyan, C.A., Schummers, J., Van Wart, A., Kuhlman, S.J., Wilson, N.R., Huang, Z.J., and Sur, M. (2010). Response features of parvalbumin-expressing interneurons suggest precise roles for subtypes of inhibition in visual cortex. Neuron *67*, 847–857.

Sakurai, T., and Okada, Y. (1992). Selective reduction of glutamate in the rat superior colliculus and dorsal lateral geniculate nucleus after contralateral enucleation. Brain Res. *573*, 197–203.

Scholpp, S., and Lumsden, A. (2010). Building a bridal chamber: development of the thalamus. Trends Neurosci. *33*, 373–380.

Sillito, A.M., and Kemp, J.A. (1983). The influence of GABAergic inhibitory processes on the receptive field structure of X and Y cells in cat dorsal lateral geniculate nucleus (dLGN). Brain Res. *277*, 63–77.

Southwell, D.G., Froemke, R.C., Alvarez-Buylla, A., Stryker, M.P., and Gandhi, S.P. (2010). Cortical plasticity induced by inhibitory neuron transplantation. Science *327*, 1145–1148.

Spitzer, N.C. (2006). Electrical activity in early neuronal development. Nature *444*, 707–712.

Stafford, B.K., Sher, A., Litke, A.M., and Feldheim, D.A. (2009). Spatial-temporal patterns of retinal waves underlying activity-dependent refinement of retinofugal projections. Neuron *64*, 200–212.

Sugiyama, S., Di Nardo, A.A., Aizawa, S., Matsuo, I., Volovitch, M., Prochiantz, A., and Hensch, T.K. (2008). Experience-dependent transfer of Otx2 homeoprotein into the visual cortex activates postnatal plasticity. Cell *134*, 508–520.

Sun, C., Warland, D.K., Ballesteros, J.M., van der List, D., and Chalupa, L.M. (2008). Retinal waves in mice lacking the beta2 subunit of the nicotinic acetylcholine receptor. Proc. Natl. Acad. Sci. USA *105*, 13638–13643.

Suzuki-Hirano, A., Ogawa, M., Kataoka, A., Yoshida, A.C., Itoh, D., Ueno, M., Blackshaw, S., and Shimogori, T. (2011). Dynamic spatiotemporal gene expression in embryonic mouse thalamus. J. Comp. Neurol. *519*, 528–543.

Tamamaki, N., Yanagawa, Y., Tomioka, R., Miyazaki, J., Obata, K., and Kaneko, T. (2003). Green fluorescent protein expression and colocalization with calretinin, parvalbumin, and somatostatin in the GAD67-GFP knock-in mouse. J. Comp. Neurol. *467*, 60–79.

Toyoda, R., Assimacopoulos, S., Wilcoxon, J., Taylor, A., Feldman, P., Suzuki-Hirano, A., Shimogori, T., and Grove, E.A. (2010). FGF8 acts as a classic diffusible morphogen to pattern the neocortex. Development *137*, 3439–3448.

Triplett, J.W., Owens, M.T., Yamada, J., Lemke, G., Cang, J., Stryker, M.P., and Feldheim, D.A. (2009). Retinal input instructs alignment of visual topographic maps. Cell *139*, 175–185.

Tucker, P., Laemle, L., Munson, A., Kanekar, S., Oliver, E.R., Brown, N., Schlecht, H., Vetter, M., and Glaser, T. (2001). The eyeless mouse mutation (ey1) removes an alternative start codon from the Rx/rax homeobox gene. Genesis *31*, 43–53.

Vue, T.Y., Aaker, J., Taniguchi, A., Kazemzadeh, C., Skidmore, J.M., Martin, D.M., Martin, J.F., Treier, M., and Nakagawa, Y. (2007). Characterization of progenitor domains in the developing mouse thalamus. J. Comp. Neurol. *505*, 73–91.

Wang, Y., Li, G., Stanco, A., Long, J.E., Crawford, D., Potter, G.B., Pleasure, S.J., Behrens, T., and Rubenstein, J.L.R. (2011a). CXCR4 and CXCR7 have distinct functions in regulating interneuron migration. Neuron *69*, 61–76.

Wang, X., Sommer, F.T., and Hirsch, J.A. (2011b). Inhibitory circuits for visual processing in thalamus. Curr. Opin. Neurobiol. *21*, 726–733.

Wang, X., Vaingankar, V., Sanchez, C.S., Sommer, F.T., and Hirsch, J.A. (2011c). Thalamic interneurons and relay cells use complementary synaptic mechanisms for visual processing. Nat. Neurosci. *14*, 224–231.

Wenner, P. (2011). Mechanisms of GABAergic homeostatic plasticity. Neural Plast. *2011*, 489470.

Williams, S.R., Turner, J.P., Anderson, C.M., and Crunelli, V. (1996). Electrophysiological and morphological properties of interneurones in the rat dorsal lateral geniculate nucleus in vitro. J. Physiol. *490*, 129–147.

Wortham, M., Jin, G., Sun, J.L., Bigner, D.D., He, Y., and Yan, H. (2012). Aberrant Otx2 expression enhances migration and induces ectopic proliferation of hindbrain neuronal progenitor cells. PLoS ONE *7*, e36211.

Xu, H.-P., Furman, M., Mineur, Y.S., Chen, H., King, S.L., Zenisek, D., Zhou, Z.J., Butts, D.A., Tian, N., Picciotto, M.R., and Crair, M.C. (2011). An instructive role for patterned spontaneous retinal activity in mouse visual map development. Neuron *70*, 1115–1127.

Zhang, J., Ackman, J.B., Xu, H.-P., and Crair, M.C. (2012). Visual map development depends on the temporal pattern of binocular activity in mice. Nat. Neurosci. *15*, 298–307.